

RESEARCH ARTICLE

Textile-based triboelectric nanogenerators integrated with 2D materials

Iftikhar Ali¹ | Nazmul Karim^{1,2}  | Shaila Afroj^{1,3}

¹Centre for Print Research (CFPR),
The University of the West of England,
Bristol, UK

²Nottingham School of Art and Design
(NSAD), Nottingham Trent University,
Nottingham, Nottinghamshire, UK

³Faculty of Environment, Science and
Economy, Department of Engineering,
University of Exeter, Exeter, UK

Correspondence

Nazmul Karim, Nottingham School of Art
and Design (NSAD), Nottingham Trent
University, Shakespeare Street,
Nottingham NG1 4GG, UK.

Email: nazmul.karim@ntu.ac.uk

Shaila Afroj, Faculty of Environment,
Science and Economy, Department of
Engineering, University of Exeter, Exeter,
EX4 4QF, UK.

s.afroj@exeter.ac.uk

Funding information

UKRI Research England the Expanding
Excellence in England (E3)

Abstract

The human body continuously generates ambient mechanical energy through diverse movements, such as walking and cycling, which can be harvested via various renewable energy harvesting mechanisms. Triboelectric Nanogenerator (TENG) stands out as one of the most promising emerging renewable energy harvesting technologies for wearable applications due to its ability to harness various forms of mechanical energies, including vibrations, pressure, and rotations, and convert them into electricity. However, their application is limited due to challenges in achieving performance, flexibility, low power consumption, and durability. Here, we present a robust and high-performance self-powered system integrated into cotton fabric by incorporating a textile-based triboelectric nanogenerator (T-TENG) based on 2D materials, addressing both energy harvesting and storage. The proposed system extracts significant ambient mechanical energy from human body movements and stores it in a textile supercapacitor (T-Supercap). The integration of 2D materials (graphene and MoS₂) in fabrication enhances the performance of T-TENG significantly, as demonstrated by a record-high open-circuit voltage of 1068 V and a power density of 14.64 W/m² under a force of 22 N. The developed T-TENG in this study effectively powers 200+ LEDs and a miniature watch while also charging the T-Supercap with 4-5 N force for efficient miniature electronics operation. Integrated as a step counter within a sock, the T-TENG serves as a self-powered step counter sensor. This work establishes a promising platform for wearable electronic textiles, contributing significantly to the advancement of sustainable and autonomous self-powered wearable technologies.

KEYWORDS

2D materials, e-textiles, energy harvesting, smart materials, textile, wearable technology

1 | INTRODUCTION

Wearable electronic textiles (e-textiles) and the Internet of Things (IoT) have encouraged extraordinary

developments, stimulating advances in biosensors, smart wearable systems, and cutting-edge solutions for health-care and portable electronics.¹⁻³ The rise in the number of sensors in e-textile devices promptly correlates with an

This is an open access article under the terms of the [Creative Commons Attribution](https://creativecommons.org/licenses/by/4.0/) License, which permits use, distribution and reproduction in any medium, provided the original work is properly cited.

© 2024 The Author(s). *EcoMat* published by The Hong Kong Polytechnic University and John Wiley & Sons Australia, Ltd.

increase in power demand. However, existing power sources, such as rechargeable or electrochemical batteries, are not only rigid and bulky but also suffer from short lifespans, posing significant barriers to the scalability of wireless sensors and wearable devices.^{4–6} There remains a need for a sustainable, flexible, wearable and durable power source for wearable e-textiles.^{7,8} Furthermore, the rapid trend towards miniaturization, as well as the growing emphasis on wearability in portable electronics, needs a fundamental re-evaluation of both design principles and operational requirements.^{9,10}

Triboelectric nanogenerator (TENG) stands out as one of the most promising emerging renewable energy harvesting technologies for wearable applications.¹¹ Such devices are capable of harnessing diverse forms of mechanical energy like vibrations, pressure, and rotations, and converting them into electricity.^{12–15} Triboelectric charges build on the surfaces where two different materials with dissimilar electron affinities meet under mechanical stress or deformation, resulting in the generation of a potential difference between the two electrodes and can be utilized directly to power electronics like LEDs or mini watches.^{16,17} Additionally, the electricity generated can be stored in electrochemical batteries or supercapacitors, enabling the operation of various portable devices.¹⁸ Textile-based TENGs have recently emerged as self-powered sources for e-textile applications, attracting considerable attention due to its lightweight, flexible and wearable nature.^{19–21} However, their low power-generating capabilities indicate ample opportunity for further development in creating self-sufficient power sources for wearable e-textiles.²²

Recently, there has been a significant focus on two-dimensional (2D) materials in the development of diverse energy harvesting devices.³ The versatile role of these materials encompasses their utilization as electrodes, buffer layers, and performance enhancers, notably in terms of efficiency and durability.²³ Moreover, the application of 2D materials in the development of TENGs has attracted significant attention, with various 2D materials being employed to augment the performance of these devices.²⁴ Significant progress has been made in the development of wearable TENG devices based on 2D materials. However, notable challenges persist, particularly concerning the poor durability and stability of these devices.²⁵ Additionally, research on textile-based TENGs using 2D materials for self-power applications remains lacking, highlighting the critical need for focused studies aimed at enhancing both the lifespan and power generation capabilities of textile-based TENGs.

Here we report the development and utilization of a textile-based self-powered system, combining both T-TENG and T-Supercap. The primary objective revolves

around enhancing the output efficiency of T-TENG through the integration of 2D materials, notably utilizing graphene as electrodes and introducing 2D MoS₂ to augment device performance. The pivotal use of triboelectricity insulator-coating materials (positive) in tandem with thin Kapton tape (negative) facilitates the crucial triboelectricity process. In the textile-based supercapacitor realm, graphene serves as the principal electrode, complemented by an ionic electrolyte. The resultant T-TENG device showcases a remarkable capability, generating an excess of 1068 V in open circuit voltage (V_{OC}), illuminating more than 200 commercial LEDs interconnected in a series configuration. Furthermore, the T-TENG is capable of charging nine T-Supercaps in series to 10 V in 250 s employing a 7–10 N force and a frequency of 4–6 Hz. Notably resilient, the device sustains over 45% of its outputs even after a continuous operation span of 7 months. Moreover, when affixed to diverse body parts, it exhibits a potential to generate over 482 V V_{OC} during walking, demonstrating its viability for practical integration within wearable technologies.

2 | RESULTS AND DISCUSSION

2.1 | System overview and working mechanism of T-TENG

In this tech-driven era, imagine harvesting ambient energy from human motion to power wearable devices like a cyclist's shirt with built-in energy harvesting and storage system (Figure 1A). This approach eliminates complex circuits, promising cost-effective maintenance and paving the way for a more sustainable energy solution for wearable sensors and portable electronics. A comprehensive overview of the T-TENG configurations used in this study and their working mechanisms is presented in Figure 1B. The proposed T-TENGs operate on contact separation mode based on the triboelectric effect, where two dissimilar materials with different electron affinities generate opposite charges when they come into contact. These charges are then collected through electrodes and recombined after passing through a load. Similarly, when force is applied to the T-TENG device, where during a pressing mode, a high peak is generated. Each step in Figure 1B corresponds to an illustrated output in Figure 1C. This peak returns to 0 as long as the T-TENG tribo-layers remain pressed and in contact due to the lack of separation of charges. Upon release, a negative voltage peak occurs due to the built-in electric field among the layers. This process, demonstrated through Figure 1B,C, allows for the cyclic generation of electricity by pressing and releasing the T-TENG device.

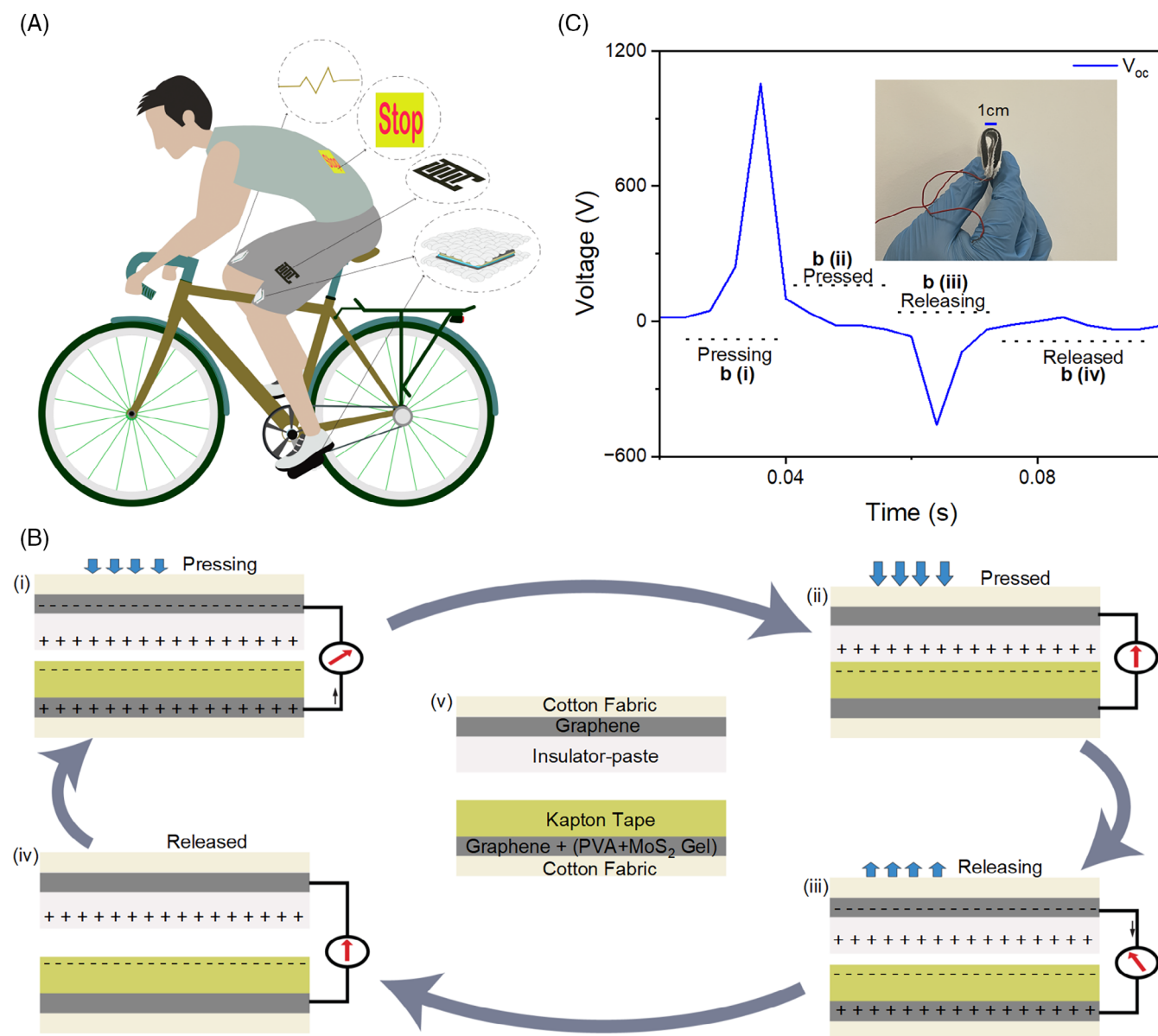


FIGURE 1 System overview and working mechanism of T-TENG; (A) Schematic illustration of integrated self-powered system, where a cyclist wearing a dress having energy harvesting (T-TENG), storage (T-Supercap) and real-time applications (Powering LEDs and counting steps). (B) Working mechanism: (i) pressing, (ii) pressed, (iii) releasing, (iv) released state and (v) the configuration of T-TENG. (C) the corresponding output curve in response to each step in (B).

2.2 | Influencing factors on output performance

The structural parameters of the T-TENG can be fine-tuned based on specific requirements, including materials, gap dimensions, layer thickness, and more. This section will first showcase how the incorporation of the 2D material (MoS₂) positively impacts performance and subsequently investigate other influential factors affecting the performance of T-TENG.²⁴ Six devices are developed with the following configuration: Fabric/Graphene/Insulator-coating (Tribo-material 1)/Spacer (sponge)/

Kapton tape (Tribo-material 2)/PVA-MoS₂ composite gel/Graphene/Fabric (Figure 2A). These devices are designed to investigate the impact of polyvinyl alcohol-MoS₂ (PVA + MoS₂) gel with varying concentrations of MoS₂ (2, 1, 0.5 and 0.1 g/L in water), as well as one device with only PVA gel and one without any gel. In the upper section of the T-TENG, graphene serves as the electrode on a cotton fabric substrate, while an insulator paste material is utilized as the positive tribo-layer. Proceeding to the bottom section of the T-TENG, a graphene electrode layer fabricated on a cotton fabric, forming a combination with a PVA + MoS₂ gel layer. This gel layer

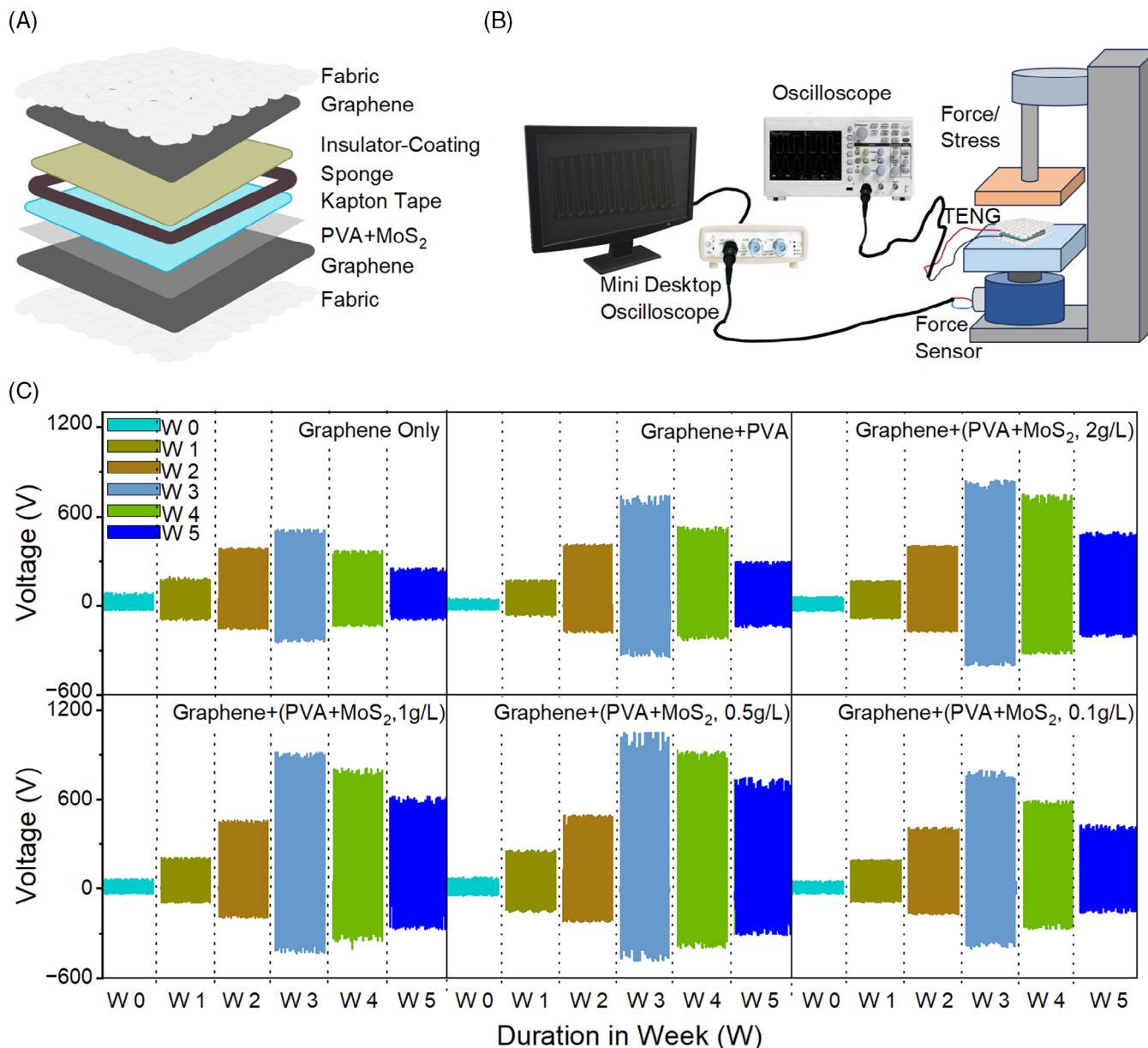


FIGURE 2 Output performance; (A) the schematic of the developed T-TENG, highlighting its diverse layers. (B) The accompanying measurement setup comprise of digital oscilloscopes for measuring the output of T-TENG, mini desktop oscilloscope for measuring the force and a force machine equipped with force measurement capabilities. (C) The output response of the developed T-TENGs subjected to a 22 N force at a frequency of 5–7 Hz, tracked from day 1st to the end of week 5. These devices exhibit variations in MoS₂ ratios while maintaining a consistent overall configuration.

incorporates varying concentrations of MoS₂, strategically designed to augment the capacity and long-term cycling performance of the graphene electrode.²⁶ Kapton tape functions both as the negative tribo-layer and an encapsulating layer. The integration of the upper and lower sections of the T-TENG is facilitated by employing a sponge as a spacer, enhancing the triboelectric effect in contact separation mode. The open-circuit voltage (V_{oc}) of these devices was characterized using a specialized stress machine assembled in the lab, equipped with

various force-exerting, and measuring capabilities, along with a digital oscilloscope (Figure 2B). The output results (V_{oc}) of these T-TENGs were obtained at weekly intervals (W), starting from the first day of fabrication and continuing until the fifth week (Figure 2C). The measurements were conducted with a frequency of 6–8 Hz and a force of 20–22 N. The results consistently showed improvement until week 3 (W3) due to several factors. The repeated application of force resulted in a tighter contact between the tribo-layer and the conductive

electrode (graphene), promoting stronger bonding and higher charge accumulation. As time passed, the drying of the layers reduced internal charge recombination, positively influencing the output results. However, a decline in performance was noted after week 4 (W4). This decrease was attributed to issues such as the residual adhesiveness of Kapton tape leaving contamination on the graphene layer, leading to reduced adhering and reduced charge accumulation.²⁷ Additionally, continuous bending and stress caused surface cracks that confirm from scanning electron microscopy (SEM) images, elevating sheet resistance and parasitic capacitance and further decreasing the output results (Figure S1–2, supporting information). Additionally, the environmental humidity also impacts the device's performance by facilitating the adherence of water molecules to the triboelectric surface. This adherence leads to the dissipation of charge, thereby reducing the charge density on the material surface and consequently compromising the device's output performance.²⁸ However, Despite these challenges, the decreasing ratio with time is observed smaller after W5, and even after 7 months, these devices still retain the ability to generate around 45% of the peak results achieved after W3 (Figure S3, supporting information), demonstrating the high durability of the fabricated T-TENG.

As illustrated in Figure 2C, the incorporation of MoS₂ significantly improved the output performance of the T-TENG device. A comparison of the inclusion of PVA gel to that of only graphene electrodes is studied and observed an elevation of 17.67% increase in the output results compared to that of graphene only. The boosted results can be due to PVA's strong dielectric characteristics, which successfully increased the surface's tribo-positive polarity.²⁹ Similarly, the addition of MoS₂ at a concentration of 0.1 g/L in composition with PVA in a ratio of 1:1 (PVA + MoS₂, 0.1 g/L) resulted in 21.31% improvement in output performance compared to the T-TENG with only graphene. Moreover, elevating the concentration of MoS₂, particularly at 0.5 g/L in the composite (PVA + MoS₂, 0.5 g/L), enhanced the device performance significantly, demonstrating an improvement of approximately 34.94% compared to T-TENG solely incorporating graphene, and 18.40% increase compared to that T-TENG based on only the PVA layer on the graphene electrode. T-TENGs with further higher concentrations of MoS₂ such as 1 g/L and 2 g/L, generated high voltages compare to those without MoS₂. However, their output voltages remained below that of T-TENG containing a 0.5 g/L MoS₂ concentration. This observation is likely linked to the inherent characteristics of the 2D material MoS₂.³⁰ Initially, the quantity of MoS₂ impacts the electrochemical properties of the graphene-MoS₂ composite electrode. While a high MoS₂

concentration decreases electrical conductivity, it also leads to the aggregation of MoS₂ on the graphene layer. Conversely, a low MoS₂ concentration contributes less to the overall capacity and graphene accumulation, thereby affecting the output results.³⁰ Consequently, achieving a balance in concentration emerged as a crucial factor in our study, ultimately yielding an optimized voltage of approximately 1068 V with a 0.5 g/L MoS₂ concentration.

Following material optimization, structural optimization was undertaken to augment the T-TENG output response. A T-TENG device was constructed with PVA + MoS₂ (0.5 g/L) on both sides. The T-TENG device with one side PVA + MoS₂ (0.5 g/L) performed better than the T-TENG with two sides PVA + MoS₂ (0.5 g/L) by about 8.87% (Figure 3A). This difference might explain the similarities in the composition of both electrodes since the major goal of the composite PVA + MoS₂ gel was to improve the triboelectric effect and aid in charge separation. With comparable compositions on both sides, a comparatively weak electric field is established within T-TENG and leading in reduced overall output performance.³¹ The investigation further explored optimizing the performance of T-TENG by exploring the potential impact of tribo-layer thickness. Varied thicknesses of insulator-coating materials (tribo-layer) were examined, revealing an optimal thickness of approximately 570 μm . Intriguingly, further increases in thickness led to a decline in T-TENG performance (Figure 3B). This phenomenon arises when the thickness exceeds an optimal point, leading to a decrease in surface charge density. The performance of a TENG relies significantly on this surface charge density, which is influenced by the dielectric layer's thickness. Hence, fine-tuning the thickness of dielectric layers can enhance the overall performance of a TENG device.³² The performance of TENGs relies significantly on the distance or space between tribo-layers. To determine the optimal spacer thickness for our T-TENG, we varied the thickness from 1 to 12 mm. The observations revealed a notable enhancement in output voltage with increasing spacer (sponge) thickness, reaching a peak at 5.5 mm. However, a further increase in spacer thickness resulted in a decline in output voltage. Thus, the findings depicted in Figure 3C demonstrate the critical importance of selecting an optimum spacer thickness, a notion supported by various studies.⁴ To determine the influence of active area on the performance of the device, T-TENGs were constructed with four different active areas and subjected to a 22 N force. A linear increasing trend in the output was observed, as the active areas were progressively enlarged (Figure 3D). The developed T-TENGs demonstrated exceptional endurance, withstanding characterization under a 14 N strain for more than 1000 cycles. Throughout testing, the output

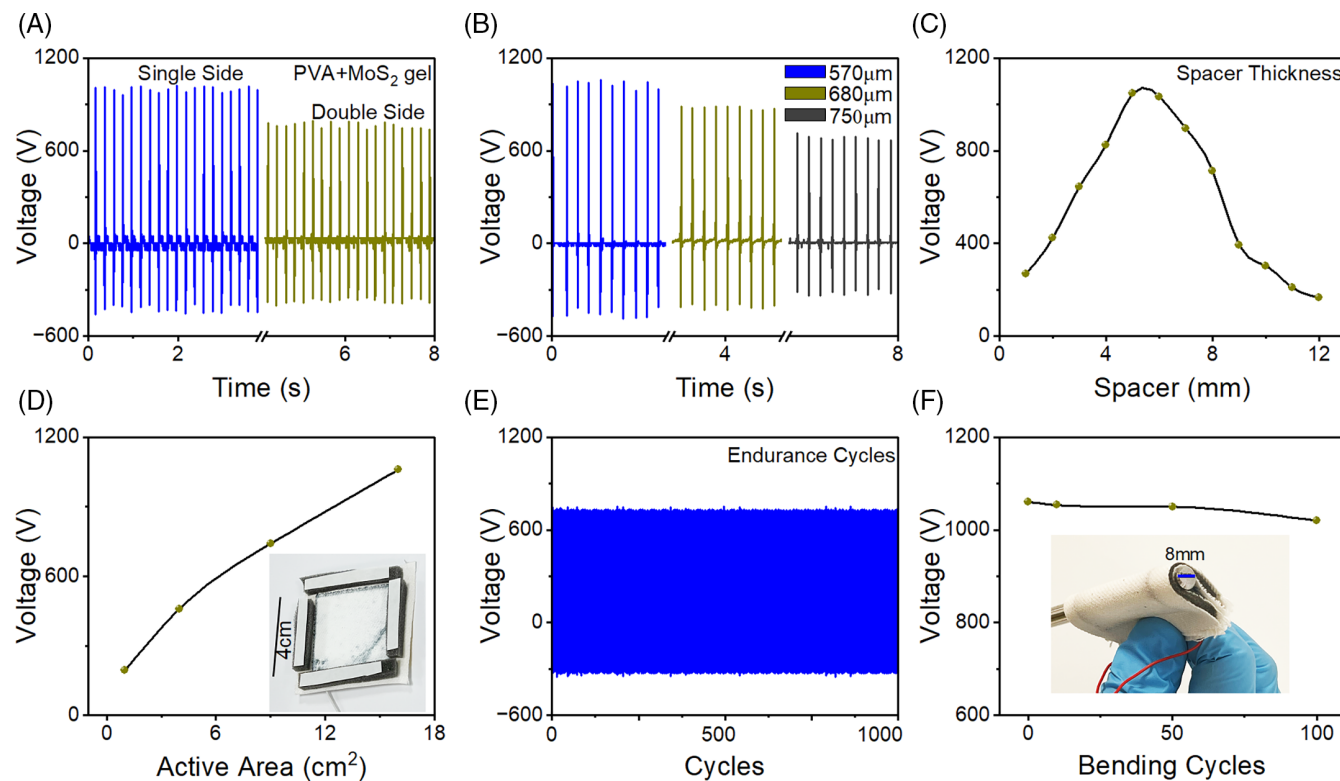


FIGURE 3 The further optimization of the T-TENG involved various aspects: (A) exploration of single-sided and double-sided PVA + MoS₂ (0.5% wt.), (B) variation in the thickness of the insulator-coating layer (tribo-layer), (C) examination of the effect of spacer size on output, (D) investigation of the response of output with increasing T-TENG activation, with the inset displaying the active area of the T-TENG top section, (E) endurance testing of the T-TENG device through approximately 1000 cycles under a 14 N force with a frequency of 5–7 Hz, and (F) a demonstration of flexibility through 100 bending cycles with an 8 mm radius of curvature, as illustrated in the inset photo of the T-TENG bending around an 8 mm diameter rod.

displayed steady performance with barely any decline (Figure 3E). To test wearability and flexibility, the devices were bent with an 8-mm radius of curvature, and the devices retained an amazing 96% of their output even after 100 bending cycles (Figure 3F). These findings highlight the T-TENG device's potential for usage in a variety of long-term applications, notably in wearable technologies.

2.3 | Electrical performance of the optimized T-TENG

The optimisation of the T-TENG results in a final design that includes MoS₂ on one side and a 5.5 mm thick spacer. The tribo-layer, composed of an insulator-coating material, is kept at an optimal thickness of 57 μm. The V_{oc} of the optimized T-TENG was explored in relation to different forces to assess its potential for integration into diverse wearable positions like elbow joints and shoes or socks. Increasing the force on the T-TENG led to a significant rise in output voltage, with the device achieving an output

voltage exceeding 1070 V at a force of 22 N (Figure 4A). Additionally, the response of the T-TENG to various frequencies was investigated using a 10 N force, revealing a slight increase in output voltage with frequency. An increase of 1.2 times was observed up to 8 Hz compared to 1 Hz, but there was very minor increase above 9 Hz (Figure 4B). These results emphasize the T-TENG's potential for implementation in various wearable applications, offering the ability to harvest energy during activities such as walking, running, cycling, and more.

The optimized T-TENG was subjected to further characterization under various resistive loads, revealing a rectified output voltage of approximately 1028 under a 22 N force across a 50 MΩ and current of approximately 20.2 μA (Figure 4C,D). The power density was computed and found around 14.64 W/m² (Figure 4E). Numerous studies have found encouraging findings for textile-based triboelectric nanogenerators (TENGs). Notably, the findings of this study stand out as having the highest reported values among cotton fabric-based TENGs. To support these findings, a comparison table (Table 1) is presented, which includes results from previously published

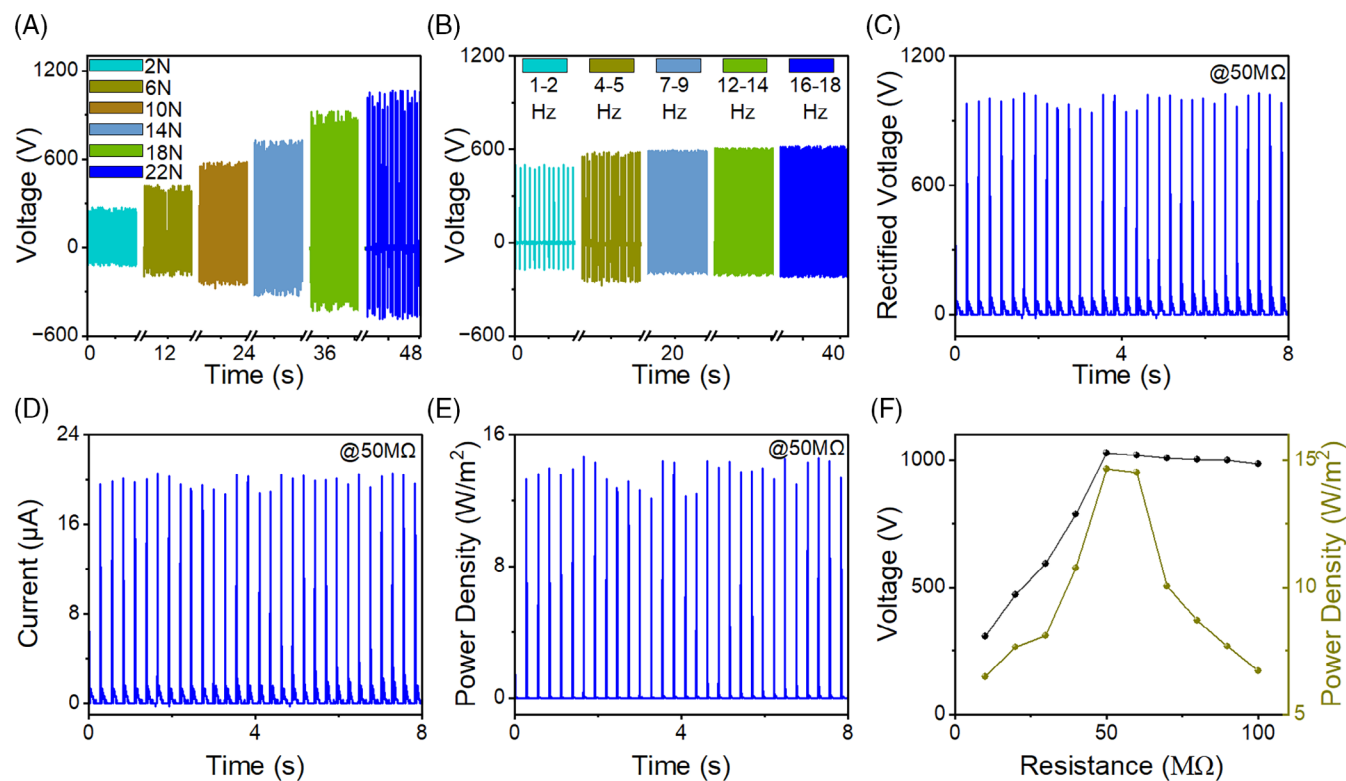


FIGURE 4 Output performance of optimized T-TENG; (A) Open circuit voltage in response to varying force, and (B) with varying frequency under 14 N force. Rectified outputs at 50 M Ω resistive load (C) Voltage, (D) Current, and (E) power density. (F) the output voltages and power densities response to various resistive loads from low to high.

TABLE 1 Performance comparison with recently published textile-based TENGs.

| Materials/substrates | V_{oc} (V) | Power density (W/m ²) | Year/Ref |
|--|--------------|-----------------------------------|---------------------|
| Woven conductive textile, Si-rubber, silk, knitted conductive textile | 28.13 | 0.166 | 2017, ³³ |
| Black phosphorus, cellulose-derived hydrophobic nanoparticles, PET fabric | 880 | 5.2 | 2018, ³⁴ |
| Nylon fabric, Ag electrodes, fabric, acrylic, polyvinyl chloride | 136 | 0.0388 | 2019, ³⁵ |
| Fluorinated ethylene propylene, nylon, Ag, tape | 120 | 0.0465 | 2019, ³⁶ |
| Cyanoalkyl silane, fluoroalkyl silane, silver, cotton, silk | 216.8 | 3.45 | 2021, ³⁷ |
| Wrap Ag electrode, polytetrafluoroethylene vinyl fabric, nylon fabric | 62.9 | 0.0053 | 2022, ³⁸ |
| Graphene, polydimethylsiloxanes, polyamide textile, PET substrate | 71 | 0.0308 | 2023, ³⁹ |
| Copper wires, acetate cloth, Yarn, Ecoflex | 361.4 | 0.792 | 2023, ⁴⁰ |
| Ag-absorbed cotton, Cu-plated cotton, pristine cotton, plant fiber | 25 | 0.7225 | 2023, ⁴¹ |
| Graphene, MoS ₂ , insulator-coating, Kapton tape, cotton fabric | 1068 | 14.64 | This work |

publications on T-TENGs. Investigating the T-TENG's response to different resistive loads, measurements of rectified voltage and power densities were conducted across a range from 1 to 100 M Ω . A linear increase in both power densities and voltage was observed up to 50 M Ω ; however, a further increase in the load led to reduction in power densities (Figure 4F). These characterizations demonstrate the potential of T-TENGs for applications requiring high loads.

2.4 | Energy storage unit: Textile supercapacitors

As part of making a fully self-powered energy system, an energy storage unit was achieved through the development of in-plane symmetrical textile-based supercapacitors (three in series), utilizing graphene as the electrode material and PVA gel as the electrolyte. Each individual supercapacitor comprises three branches, each having a

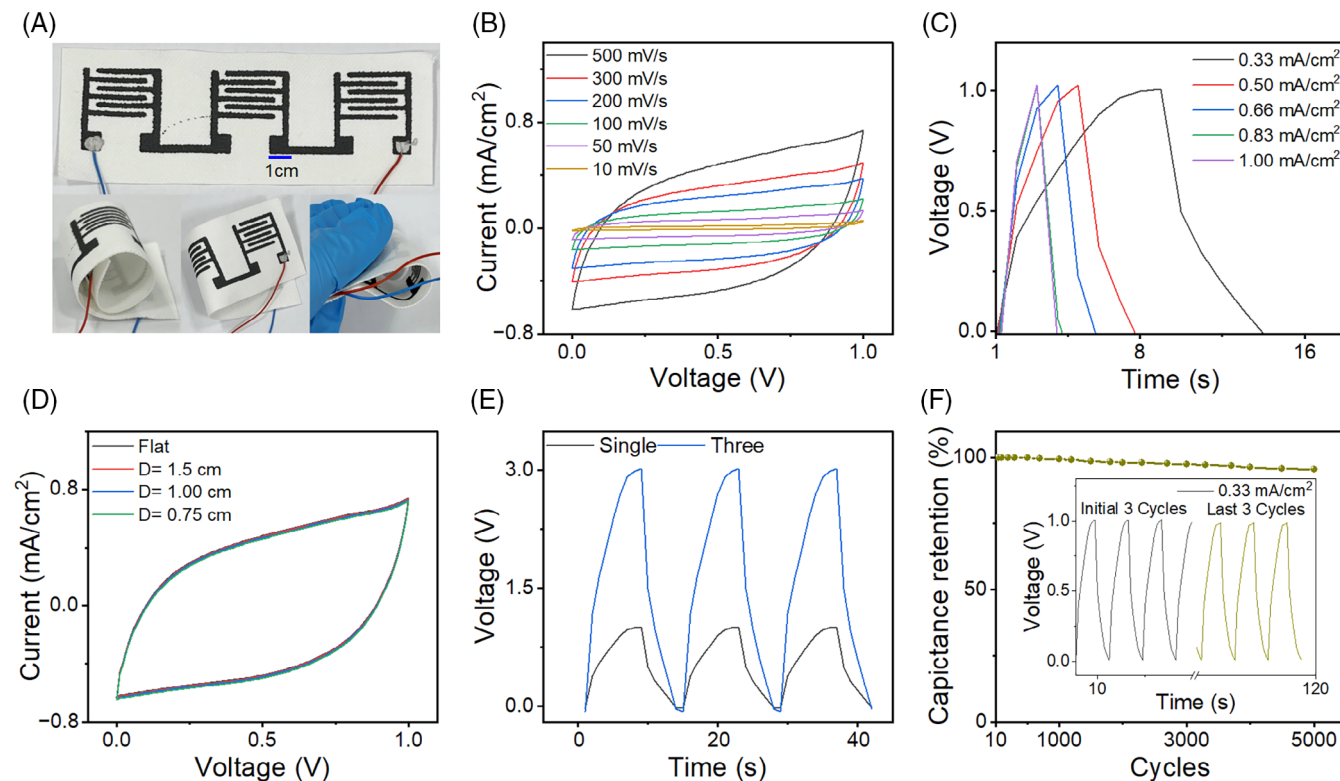


FIGURE 5 Energy storage unit; (A) photographs of textile-based supercapacitors, where three symmetric supercapacitors in series in flat and various bending shapes. (B) CV curves for various scan rates and (C) GCD curves with various current densities. (D) CV curves were recorded with a scan rate of 500 mV/cm² under flat and three different bending radii. (E) GCD curves of single and three supercapacitors connected in series, and (F) the capacitance retentions after various cycles, while inset shows the initial and final three GCD cycles.

length of 22.6 mm and a width of 1 mm on both the anode and cathode, separated by a 1 mm gap from neighboring electrodes. A photograph of the fabricated device highlights three textile-based symmetric-type supercapacitors arranged in series with differing bending shapes that showcase the flexibility of the devices, as illustrated in Figure 5A. The electrochemical performance of the fabricated T-Supercaps was assessed through cyclic voltammetry (CV) and galvanometric charge–discharge (GCD) analyses. CV curves, obtained at various scan rates (500–10 mV/s) for a single supercapacitor, consistently exhibited rectangular shapes, indicating the T-Supercap's quality resembled that of an ideal double-layer supercapacitor (Figure 5B). In accordance with CV results, GCD for the developed T-Supercap was measured across current densities from 0.33 to 1.0 mA/cm², revealed triangular-shaped curves with nearly identical charge and discharge times, akin to an ideal double-layer supercapacitor (Figure 5C). The calculated areal capacitance for a scan rate of 10 mV/s was found to be 4.9 mF/cm², which is more than the recently published results by our group in ref.⁴² To showcase the flexibility and stability of the device, the CV curves of the supercapacitor were measured while bending at various radius of curvature. Negligible effects were observed compared to the flat

mode, indicating that the developed textile supercapacitor can be effectively employed for wearable applications in various positions on clothing (Figure 5D). To assess the electrical combination response of the developed T-Supercaps, GCD curves were recorded for both a single supercapacitor and three supercapacitors in series. It was observed that for an equivalent charging time, the three supercapacitors in series reached 3 V, while a single T-Supercap charged up to 1 V. This confirms the linear and consistent behavior in the fabricated supercapacitors, as illustrated in Figure 5E. The durability of the developed T-Supercap was validated by a cyclic run of GCD with a current density of 0.33 mA/cm² for over 1000 cycles. A minor reduction was observed, maintaining more than 96% capacitance retention (Figure 6F). These results highlight the potential of the developed T-Supercap for efficient energy storage applications.

2.5 | Integrated self-powered system: Applications

Finally, the practical applications of T-TENG and textile supercapacitors were explored. Figure 6A illustrates a schematic for charging the developed textile

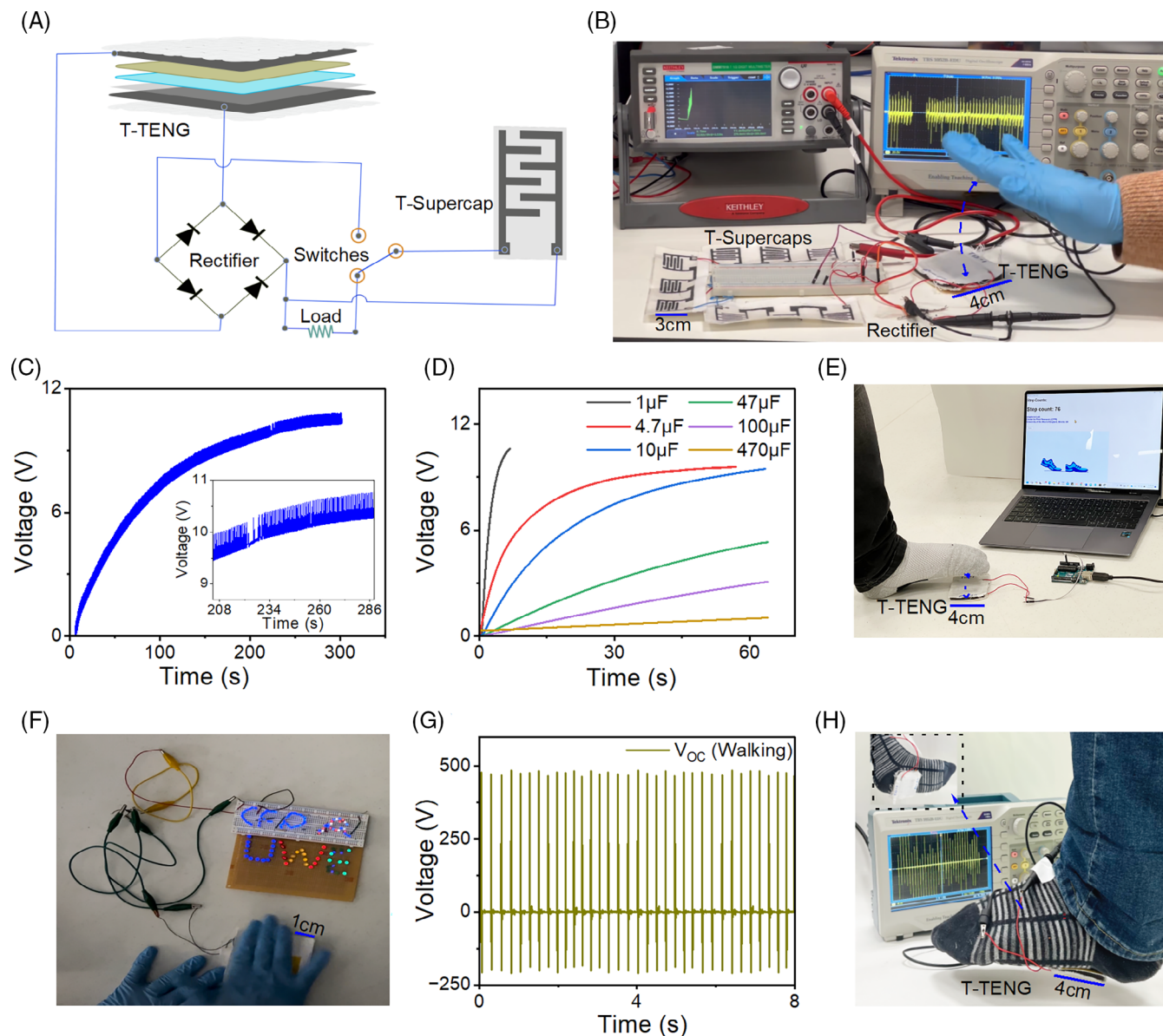


FIGURE 6 Integrated self-powered system and real-time applications; (A) Schematic of charging setup for textile supercapacitor via T-TENG and (B) photograph of textile supercapacitors connected in series while charging with T-TENG. (C) The charging curve of the Textile supercapacitors connected in series with T-TENG. (D) The charging curves of commercial supercapacitors via T-TENG. (E) A photograph of the step counting setup and (F) a photograph of LEDs glowing while hand tapping T-TENG. (G) Output voltages during fixing while fixing T-TENG on socks and (H) photograph of the T-TENG fixed on socks.

supercapacitors via T-TENGs. The T-TENG output is rectified through rectifier circuits and then supplied to T-Supercaps. The system, as captured in the photograph (Figure 6B), features nine T-Supercaps connected in series and being charged with a T-TENG through hand tapping. Figure 6C displays the charging curve of the series-connected textile supercapacitors, while a corresponding video clip, (Clip 1, supporting information), is included in the supporting information. The charging process to reach 10 volts took approximately 250 seconds, utilizing a force of 7–10 N and a frequency of 4–6 Hz.

Additionally, T-TENGs were utilized to charge commercial DC capacitors with values ranging from 1 to 470 μF , applying forces and frequencies of 8–10 N and 5–7 Hz, respectively. The T-TENG demonstrated a rapid charging capability, taking about 6 seconds to charge a 1 μF capacitor up to 10 V and approximately 60 s for a 470 μF capacitor (Figure 6D). Furthermore, T-TENGs were effectively employed with hand tapping to charge a 4.7 μF capacitor, showcasing their potential for charging small portable electronics (Clip 2, supporting information). In addition to its energy storage applications, the T-TENG

was harnessed for real-time step counting while walking or running, as seen in Figure 6E (Clip 3, supporting information). Its versatility was further demonstrated by illuminating indicators while cycling or walking, successfully lighting up over 160 commercial LEDs with just hand tapping, as showcased in Figure 6F (Clip 4, supporting information). Moreover, when placed and fixed in socks, the T-TENG generated an open-circuit voltage of approximately 480 V during walking (Figure 6G,H). This voltage output proved sufficient to power indicators with more than 120 LEDs while walking (Clip 5, supporting information).

3 | CONCLUSION

This systematic exploration into the application of 2D materials in textile-based energy harvesting and storage devices has resulted in the development of a highly efficient textile-based triboelectric nanogenerator (T-TENG). Leveraging 2D materials like graphene for electrodes and MoS₂ to enhance triboelectric performance, the optimized concentration of 0.5 g/L in water demonstrated a substantial 2.5-fold improvement in output compared to T-TENG without MoS₂. The device showcased exceptional flexibility and durability, sustaining 45% of its original performance even after 6 months. Complementing this, a textile-based supercapacitor for charge storage was created, effectively powering mini-electronics. The T-TENG also served as a step counter sensor and a reliable power source for LEDs, enabling real-time indications while walking or cycling. This self-powered system, developed on bare cotton textiles, opens avenues for the exploration of wearable e-textile applications, and marks significant attention to further explore sustainable energy solutions.

4 | EXPERIMENTAL SECTION

4.1 | Materials

Graphene (screen-printable ink) and MoS₂ dispersion in water, both with a concentration of 100 g/L, were purchased from Versarien™ plc, UK, sulfuric acid (H₂SO₄) (puriss, 95%–97%) and PVA (molecular weight: 31000–50 000, 98%–99% hydrolysed) were purchased from Merck, UK. The cotton fabric, featuring a construction of (66 × 44/70 × 10) × 340, was kindly donated by Square Apparels Limited, Bangladesh. The screen-printable insulator-coating materials (DM-IN-2510) with the dielectric constant 3.3 at 1 KHz were acquired from

Dycotec Materials Ltd (UK), while Kapton tape (25.4 μm thick) was obtained from DigiKey UK.

4.2 | T-TENG fabrication

Graphene was printed on cotton fabric as electrodes in a 4 cm by 4 cm pattern using a manual screen printer with a 63 T mesh. After printing, it was dried in an 80°C in a furnace for 10 min. Copper wires were then attached to the electrodes using silver paste. To make different concentrations of 2, 1, 0.5, and 0.1 g/L, the MoS₂ mixture was mixed with deionized water and stirred for 2 h under ambient conditions. A PVA gel was prepared by dissolving in DI water with a concentration of 100 g/L. The dispersion underwent thorough stirring for 30 min at ambient temperature, after which the temperature was elevated to 80–90°C until it reached a clear solution. Then MoS₂ + PVA gel was prepared with a 1:1 ratio and stirred at 500 rpm for 3 h under 80°C. On one textile-based graphene printed electrode, 2 mL of MoS₂ + PVA gel composite was drop cast and dispersed over the graphene, which was then dried for an hour in an ambient atmosphere before being covered with Kapton tape. Insulator-coating materials were printed over the other textile-based graphene electrodes, acting as both an encapsulation and a triboelectric layer. Both sides of the T-TENGs were then joined using a sponge as a spacer and double-sided adhesive tape.

4.3 | T-Supercap fabrication

The graphene electrode was printed on a textile substrate in-plane symmetrical shape using a manual screen printer and dried for 10 min under 80°C. The PVA gel electrolyte was developed by dissolving polyvinyl alcohol (PVA) in an aqueous solution of H₂SO₄ (50 g/L). The solution was stirred constantly at room temperature for 60 min and then heated to 80°C with continues stirrer 500–700 rpm till produce a clear solution. A 1.5 mL volume of PVA gel electrolyte was drop casted over the graphene electrode and dried before being wrapped with very flexible and transparent single-sided adhesive tape.

4.4 | Characterization instrumentation

A force applicator was developed in the laboratory using CNC and 3D printing machines. It incorporates a mechanism to convert rotary motion into linear motion using a 24 V DC motor, facilitating the exertion of force on the

T-TENG. To measure the exerting force a commercial force-measuring device was utilized in parallel (Figure S4, supporting information). The output voltage was measured using a Tektronix TBS1052B oscilloscope with 40M Ω prob along with a voltage divider circuit to overcome the peak measuring limitations (Figure S4, supporting information). The current was calculated both way using ohms law ($V=IR$) from the voltage across the resistive load and with a Keithley DMM 7510 multimeter. For the electrochemical characterization of supercapacitors, an Iviumstat electrochemical interface was utilized. In the application for step counting, an Arduino UNO controller was programmed and interfaced with a desktop application developed in Python. Additionally, the surface morphology of fabricated layers was examined using an FEI Quanta 650 field emission scanning electron microscope (SEM).

AUTHOR CONTRIBUTIONS

N.K. conceived and initiated the idea of 2D material-based energy harvesting textiles including T-TENG, and together with S. A. provided guidance to I. A. to prepare experimental plan. I. A. carried out experiments and data analysis with inputs and regular supervisions from S. A. and N.K. The draft manuscript was prepared by I. A. with inputs from N. K. and S. A. All authors contributed to the writing and reviewing of the final manuscript.

ACKNOWLEDGMENTS

The authors kindly acknowledge funding from the UWE partnership PhD scheme, and UKRI Research England the Expanding Excellence in England (E3) grant. The authors also grateful for the support from Michael White and Nathan Townsend for their technical help in developing the force applicator and force measuring system, as well as David Patton for his assistance with SEM imaging.

CONFLICT OF INTEREST STATEMENT

The authors declare no conflict of interest.

ORCID

Nazmul Karim  <https://orcid.org/0000-0002-4426-8995>

REFERENCES

- Libanori A, Chen G, Zhao X, Zhou Y, Chen J. Smart textiles for personalized healthcare. *Nat Electron*. 2022;5:142. doi:10.1038/s41928-022-00723-z
- Ates HC, Nguyen PQ, Gonzalez-Macia L, et al. End-to-end design of wearable sensors. *Nat Rev Mater*. 2022;7(11):887-907. doi:10.1038/s41578-022-00460-x
- Ali I, Dulal M, Karim N, Afroj S. 2D material-based wearable energy harvesting textiles: a review. *Small Struct*. 2024;5:2300282. doi:10.1002/sstr.202300282
- Ali I, Hassan G, Shuja A. Fabrication of self-healing hybrid nanogenerators based on polyurethane and ZnO for harvesting wind energy. *J Mater Sci Mater Electron*. 2022;33:3982. doi:10.1007/s10854-021-07591-x
- Chang A, Uy C, Xiao X, Xiao X, Chen J. Self-powered environmental monitoring via a triboelectric nanogenerator. *Nano Energy*. 2022;98(107):282. doi:10.1016/j.nanoen.2022.107282
- Islam MR, Afroj S, Yin J, Novoselov KS, Chen J, Karim N. Advances in Printed Electronic Textiles. *Adv Sci*. 2024;11(6):2304140. doi:10.1002/advs.202304140
- Xiang S, Chen G, Wen Q, et al. Fully addressable textile sensor array for self-powered haptic interfacing. *Matter*. 2024;7(1):82. doi:10.1016/j.matt.2023.10.024
- Xu C, Song Y, Han M, Zhang H. Portable and wearable self-powered systems based on emerging energy harvesting technology. *Microsyst Nanoeng*. 2021;7:25. doi:10.1038/s41378-021-00248-z
- Zou J, Zhang M, Huang J, et al. Coupled supercapacitor and triboelectric nanogenerator boost biomimetic pressure sensor. *Adv Energy Mater*. 2018;8(10):1702671. doi:10.1002/aenm.201702671
- Islam MR, Afroj S, Karim N. Scalable production of 2D material heterostructure textiles for high-performance wearable supercapacitors. *ACS Nano*. 2023;17(18):481-18493. doi:10.1021/acsnano.3c06181
- Choi D, Lee Y, Lin Z-H, et al. Recent advances in triboelectric nanogenerators: from technological progress to commercial applications. *ACS Nano*. 2023;17(11):87. doi:10.1021/acsnano.2c12458
- Kwak W, Yin J, Wang S, Chen J. Advances in triboelectric nanogenerators for self-powered wearable respiratory monitoring. *FlexMat*. 2024;1(1):5. doi:10.1002/flm2.10
- Xu J, Yin J, Fang Y, et al. Deep learning assisted ternary electrification layered triboelectric membrane sensor for self-powered home security. *Nano Energy*. 2023;113(108):524. doi:10.1016/j.nanoen.2023.108524
- Fang Y, Xu J, Xiao X, et al. A deep-learning-assisted on-mask sensor network for adaptive respiratory monitoring. *Adv Mater*. 2022;34:2200252. doi:10.1002/adma.202200252
- Zhang S, Bick M, Xiao X, Chen G, Nashalian A, Chen J. Leveraging triboelectric nanogenerators for bioengineering. *Matter*. 2021;4(3):845. doi:10.1016/j.matt.2021.01.006
- Long L, Liu W, Wang Z, et al. High performance floating self-excited sliding triboelectric nanogenerator for micro mechanical energy harvesting. *Nat Commun*. 2021;12:4689. doi:10.1038/s41467-021-25047-y
- Ali I, Islam MR, Yin J, et al. Advances in smart photovoltaic textiles. *ACS Nano*. 2024;18(5):3871-3915. doi:10.1021/acsnano.3c10033
- Wen Z, Yeh M-H, Guo H, et al. Self-powered textile for wearable electronics by hybridizing fiber-shaped nanogenerators, solar cells, and supercapacitors. *Sci Adv*. 2016;2(10):e1600097. doi:10.1126/sciadv.1600097
- Yin J, Wang S, Di Carlo A, et al. Smart textiles for self-powered biomonitoring. *Med-X*. 2023;1:3. doi:10.1007/s44258-023-00001-3
- Yi J, Dong K, Shen S, et al. Fully fabric-based triboelectric nanogenerators as self-powered human-machine interactive keyboards. *Nanomicro Lett*. 2021;13(1):103. doi:10.1007/s40820-021-00621-7

21. Chen G, Xiao X, Zhao X, Tat T, Bick M, Chen J. Electronic textiles for wearable point-of-care systems. *Chem Rev.* 2022;122(3):3259. doi:10.1021/acs.chemrev.1c00502
22. Luo J, Gao W, Wang ZL. The triboelectric nanogenerator as an innovative technology toward intelligent sports. *Adv Mater.* 2021;33:2004178. doi:10.1002/adma.202004178
23. Yi F, Ren H, Shan J, Sun X, Wei D, Liu Z. Wearable energy sources based on 2D materials. *Chem Soc Rev.* 2018;47(9):3152. doi:10.1039/C7CS00849J
24. Pace G, del Rio Castillo AE, Lamperti A, Lauciello S, Bonaccorso F. 2D materials-based electrochemical triboelectric nanogenerators. *Adv Mater.* 2023;35:2211037. doi:10.1002/adma.202211037
25. Lin Z, Zhang B, Xie Y, Wu Z, Yang J, Wang ZL. Elastic-connection and soft-contact triboelectric nanogenerator with superior durability and efficiency. *Adv Funct Mater.* 2021;31:2105237. doi:10.1002/adfm.202105237
26. Teng Y, Zhao H, Zhang Z, et al. Elastic-connection and soft-contact triboelectric nanogenerator with superior durability and efficiency. *ACS Nano.* 2016;10(40):8526. doi:10.1021/acsnano.6b03683
27. Hwang H, Lee KY, Shin D, Shin J, Kim S, Choi W. Metal-free, flexible triboelectric generator based on MWCNT mesh film and PDMS layers. *Appl Surf Sci.* 2018;442:693. doi:10.1016/j.apsusc.2018.02.227
28. Li C, Bai Y, Shao J, Meng H, Li Z. Strategies to improve the output performance of triboelectric nanogenerators. *Small Methods.* 2024;2(301):682. doi:10.1002/smt.202301682
29. Uzabakirho PC, Haider Z, Emmanuel K, et al. High-performance, mechanically and thermally compliant silica-based solid polymer electrolyte for triboelectric nanogenerators application. *Adv Mater Technol.* 2020;5:2000303. doi:10.1002/admt.202000303
30. Liu C, Bai Y, Zhao Y, Yao H, Pang H. MoS₂/graphene composites: fabrication and electrochemical energy storage. *Energy Storage Mater.* 2020;33:470. doi:10.1016/j.ensm.2020.06.020
31. Pace G, Ansaldo A, Serri M, Lauciello S, Bonaccorso F. Enhancing triboelectric nanogenerators power conversion efficiency with few-layers graphene flexible electrodes. *Nano Energy.* 2020;76(104):989. doi:10.1016/j.nanoen.2020.104989
32. Hasan S, Kouzani AZ, Adams S, Long J, Mahmud MAP. Comparative study on the contact-separation mode triboelectric nanogenerator. *J Electrostat.* 2022;116(103):685. doi:10.1016/j.elstat.2022.103685
33. Choi AY, Lee CJ, Park J, Kim D, Kim YT. Corrugated textile based triboelectric generator for wearable energy harvesting. *Scientific Reports.* 2017;7(45):583. doi:10.1038/srep45583
34. Xiong J, Cui P, Chen X, et al. Skin-touch-actuated textile-based triboelectric nanogenerator with black phosphorus for durable biomechanical energy harvesting. *Nat Commun.* 2018;9(1):4280. doi:10.1038/s41467-018-06759-0
35. Paosangthong W, Wagih M, Torah R, Beeby S. Textile-based triboelectric nanogenerator with alternating positive and negative freestanding grating structure. *Nano Energy.* 2019;66(104):148. doi:10.1016/j.nanoen.2019.104148
36. Liu J, Gu L, Cui N, Xu Q, Qin Y, Yang R. Fabric-based triboelectric nanogenerators. *Research.* 2019;2019. doi:10.34133/2019/1091632
37. Sangkhun W, Wanwong S. Natural textile based triboelectric nanogenerators for efficient energy harvesting applications. *Nanoscale.* 2021;13(4):2420. doi:10.1039/d0nr07756a
38. Paosangthong W, Wagih M, Torah R, Beeby S. Textile-based triboelectric nanogenerator with alternating positive and negative freestanding woven structure for harvesting sliding energy in all directions. *Nano Energy.* 2022;92(106):739. doi:10.1016/j.nanoen.2021.106739
39. Domingos I, Saadi Z, Sadanandan KS, et al. Printed graphene electrodes for textile-embedded triboelectric nanogenerators for biomechanical sensing. *Nano Energy.* 2023;115(108):688. doi:10.1016/j.nanoen.2023.108688
40. Kim DE, Shin S, Zhang G, Choi D, Jung J. Fully stretchable textile-based triboelectric nanogenerators with crepe-paper-induced surface microstructures. *RSC Adv.* 2023;13(11):142. doi:10.1039/d3ra01032e
41. Huang J, Wang S, Zhao X, et al. Fabrication of a textile-based triboelectric nanogenerator toward high-efficiency energy harvesting and material recognition. *Mater Horiz.* 2023;10(9):3840. doi:10.1039/d3mh00618b
42. Islam MR, Afroj S, Beach C, et al. Fully printed and multifunctional graphene-based wearable e-textiles for personalized healthcare applications. *IScience.* 2022;25(3):25. doi:10.1016/j.isci.2022.103945

SUPPORTING INFORMATION

Additional supporting information can be found online in the Supporting Information section at the end of this article.

How to cite this article: Ali I, Karim N, Afroj S. Textile-based triboelectric nanogenerators integrated with 2D materials. *EcoMat.* 2024;e12471. doi:10.1002/eom2.12471